SF2A 2014
J. Ballet, F. Bournaud, F. Martins, R. Monier and C. Reylé (eds)

3C 285: A NEARBY GALAXY WITH JET-INDUCED STAR FORMATION

Q. Salomé[1], P. Salomé[1] and F. Combes[1]

Abstract. We present IRAM-30m CO observations of 3C 285, which is an example of jet-induced star formation. We observed the central galaxy and along the radio jet. The central galaxy presents a double-horn profile, which we interpret with a simple analytical model as the result of a narrow ring of disk.

In the star-forming spot (so-called 09.6), at a distance of ~ 70kpc from the galaxy, we determined an CO interesting upper limit. Plotted in a diagram of Σ_{SFR} vs Σ_{gas}, 09.6 appears to form stars at least as efficiently as typical spiral galaxies. This result supports the AGN positive feedback scenario.

Keywords: Methods:data analysis, Galaxies:evolution, interactions, star formation, Radio lines:galaxies

1 Introduction

Jet-induced star formation has been debated for decades (eg. van Breugel et al. 2004). Evidence has been found only for 4 objects: (1) Centaurus A, where the jet is encountering gas in the shells along its way (Schiminovich et al. 1994; Charmandaris et al. 2000); (2) Minkowski Object (van Breugel et al. 1985); (3) 3C 285 (van Breugel & Dey 1993); (4) at z = 3.8, the radio source 4C 41.17 (Bicknell et al. 2000; De Breuck et al. 2005; Papadopoulos et al. 2005).

3C 285 is a double-lobed powerful FR-II radio galaxy where both lobes have a complex filamentary structure. In the eastern radio lobe, there is a radio jet with unresolved radio knots. A slightly resolved object is located near the eastern radio jet (3C 285/09.6), at a projected distance of ~ 70kpc from the galaxy centre. 3C 285/09.6 is a small, kiloparsec-sized object where star formation seems to be triggered by the jet from the radio source 3C 285 (van Breugel & Dey 1993).

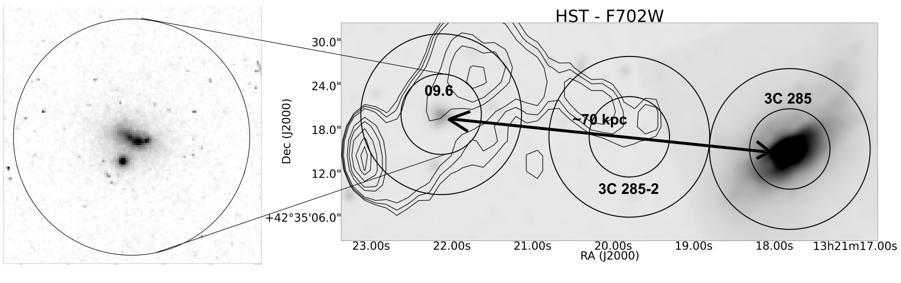

Fig. 1: Contour map of the eastern lobe of 3C 285 observed at 21 cm (van Breugel & Dey 1993) with 5″ resolution, as extracted from the VLA archive (NED, Leahy & Williams 1984), overlaid on a slightly smoothed Hα image from HST in the F702W filter (data from the HST archive, PI: Crane). The observed positions are shown by the CO(1-0) 24″ and CO(2-1) 12″ IRAM-30m beams (circles). Details of the 09.6 spot are shown in the circle on the left, and show that the spot is resolved in two or maybe three sub-structures.

To better understand the impact of the AGN interaction with the intergalactic medium on star formation, CO(1-0) and CO(2-1) have been observed along the jet axis of 3C 285 (see also Salomé et al. 2014). The observations were made with the IRAM 30m telescope on March 2014, using the EMIR receiver with the WILMA backend (bandwidth of 3.7 GHz; resolution of 2 MHz). At redshift z=0.0794, those lines are observable at frequencies of 106.780 GHz and 213.580 GHz, which leads to beams of 24″ and 12″. Three regions were observed: the central galaxy 3C285, the 09.6 spot and an intermediate position (3C 285-2) along the jet (cf. figure 1).
Our main goal was to determine whether star formation is more efficient in the shocked region along the jet. Throughout this work, we assume the cold dark matter concordance Universe, with H_0 = 70km.s^{-1}.Mpc^{-1}, Ω_m = 0.30 and Ω_Λ = 0.70.

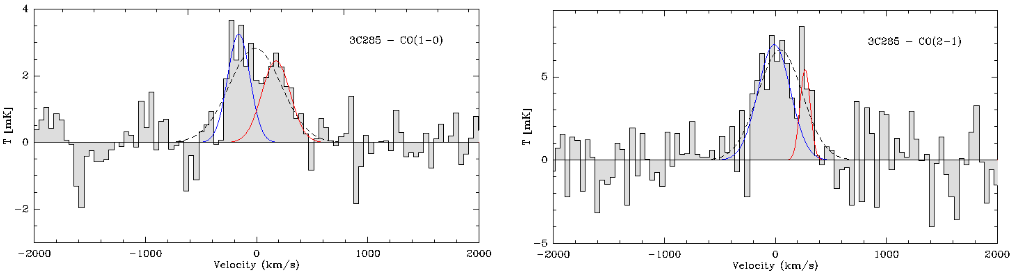

Fig. 2: *Left:* CO(1-0) spectrum for 3C 285. *Right:* CO(2-1) spectrum for 3C 285. Both spectra, are smoothed to a spectral resolution of ~ 45km/s. The dash line fits all the emission, whereas the red and blue lines fit the double-horn profile.

2 Results

CO luminosities The central galaxy 3C 285 was detected in both CO(1-0) and CO(2-1), whereas there is no detection for the other positions. Each line was fitted by a gaussian in order to get its characteristics (table 1). The CO luminosity L'_{CO} was calculated with the formula from Solomon et al. (1997). Then, the molecular gas mass was estimated from the line luminosity L'_{CO}, using a standard Milky Way conversion factor of 4.6 $M_\odot$.(K.km.s^{-1}.pc^2)$^{-1}$ (Solomon et al. 1997).

Source	line	Δv (km.s^{-1})	I_{CO} (K.km.s^{-1})	L'_{CO} (10^8 K.km.s^{-1}.pc^2)	M_{H_2} (10^9 $M_\odot$)
3C 285	CO(1-0)	553 ± 51	1.66 ± 0.15	22 ± 2	10.3 ± 0.9
	CO(2-1)	472 ± 55	3.31 ± 0.36	-	-
09.6 spot	CO(1-0)	-	< 0.100	< 1.4	< 0.62
	CO(2-1)	-	< 0.216	-	-
3C 285-2	CO(1-0)	-	< 0.159	< 2.1	< 0.99
	CO(2-1)	-	< 0.322	-	-

Table 1: Results of the observations at IRAM 30m. For non-detections, an upper limits is computed at 3σ, with a line width of Δv = 64 km.s^{-1} for 09.6 and 3C 295-2 (van Breugel & Dey 1993). More informations are given in Salomé et al. (2014).

Line width and morphology 3C 285 presents a broad line profile covering negative and positive velocities. This could result from the rotation of the galaxy around its main axis, as suggested by the apparent double-horn profile (figure 2). The double-horn profile of CO(1-0) emission is well defined, whereas it is less obvious in CO(2-1). In addition, the spectra show no kinematic effect of a molecular outflow, at the level of the 30m sensitivity.

Star formation rate and depletion time The Hα and IR emission is often used as tracers of star formation. We derived a star formation rate from the Hα (Baum & Heckman 1989; van Breugel & Dey 1993) and IR emission (computed with Herschel-SPIRE data from the archive), following the methods of Kennicutt & Evans (2012) and Calzetti et al. (2007). The total SFR is the sum of the SFR derived from the Hα and the IR emission. Table 2 summarises the SFR of the different sources (see Salomé et al. 2014 for more details). The depletion time is the time to consume all the gas with the present star formation rate: $t_{depl} \sim M_{gas}/SFR$.

Source	$SFR_{H\alpha}$	SFR_{TIR}	$SFR_{24\,\mu m}$	SFR_{total}
3C 285	1.34	19.7	12.0	21.04
09.6 spot	0.15	< 0.79	0.61	0.76

Table 2: SFR in $M_\odot$.yr^{-1} for 3C 285 and the 09.6 spot. The Hα, TIR and 24 μm SFR were calculated with Kennicutt & Evans (2012) and Calzetti et al. (2007). The total SFR is a combination of those SFR.

3 Discussion

A compact molecular ring in 3C 285 In order to interpret the kinematics of our CO data, we use a simple analytical model which computes the velocity spectrum of the galaxy (Wiklind et al. 1997). This allows to determine the gas concentration in 3C 285. For 3C 285, the half-light radius is ~ 8.3 kpc (Roche & Eales 2000), with a stellar mass of ~ 2×10^{11} $M_\odot$. The density profile derived by the model indicates that **the gas is distributed in a narrow ring** that

[1] LERMA, Observatoire de Paris, CNRS UMR 8112, 61 avenue de l'Observatoire, 75014 Paris, France

extends at distances up to ~ 3.5 kpc with an average radius ~ 1.5 kpc (for more details, refer to Salomé et al. 2014), but this need to be confirmed by interferometric data. The gas ring may be interpreted as the result of a past merger event; the gas being now in equilibrium in the ring. This phenomenon is also observed in other gas rich early-type galaxies, like in the most famous example Centaurus A.

A Kennicutt-Schmidt law? We have calculated the gas and SFR surface densities ($\Sigma_{\rm gas}$, $\Sigma_{\rm SFR}$; the values can be found in Salomé et al. 2014). For 3C 285, both quantities are smoothed over the CO(1-0) IRAM-30m beam, whereas for the 09.6 spot, the surface densities are estimated on the area of the Hα emission (in a radius of ~ 1.65″). Plotting this in the $\Sigma_{\rm SFR}$ vs $\Sigma_{\rm gas}$ diagram (see figure 3, Bigiel et al. 2008; Daddi et al. 2010), both positions follow a Schmidt-Kennicutt law $\Sigma_{\rm SFR} \propto \Sigma^{\rm N}_{\rm H_2}$ (Kennicutt 1998).

Source	$M_{\rm gas}$ ($M_\odot$)	M_* ($M_\odot$)	$f_{\rm gas}$	SFR ($M_\odot$.yr^{-1})	$t_{\rm dep}$ (Gyr)	sSFR (Gyr^{-1})
3C 285	1.03×10^{10}	4.20×10^{11}	0.025	21.04	0.49	5.0×10^{-2}
09.6 spot	$< 6.2 \times 10^{8}$	1.9×10^{9}	< 0.326	0.76	< 0.82	4.0×10^{-1}

Table 3: Molecular gas, stellar masses and gas fraction for 3C 285 and 09.6. The stellar mass of 3C 285 is given in Tadhunter et al. (2011), whereas that of 09.6 is calculated with the mass-to-light ratio (Bell & de Jong 2001). The depletion time is computed from the CO-derived gas masses and the SFR.

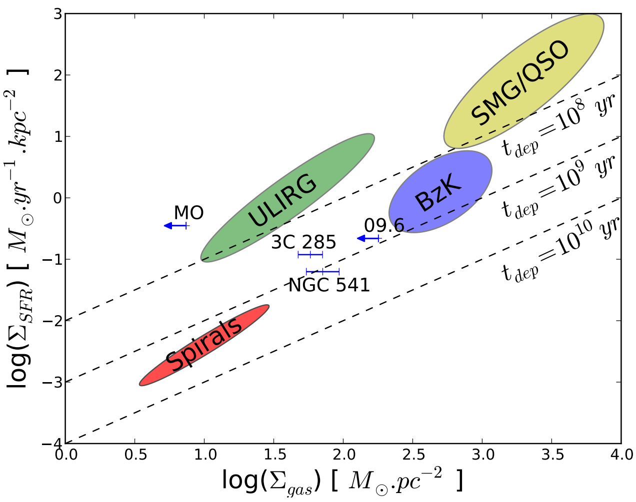

Fig. 3: $\Sigma_{\rm SFR}$ vs. $\Sigma_{\rm gas}$ diagram for the sources studied in Salomé et al. (2014). The diagonal dashed lines show lines of constant SF efficiency, indicating the level of $\Sigma_{\rm SFR}$ needed to consume 1%, 10%, and 100% of the gas reservoir in 10^8 years. Thus, the lines also correspond to constant gas depletion times of, from top to bottom, 10^8, 10^9, and 10^{10} yr The coloured regions come from Daddi et al. (2010).

As a conclusion, figure 3 shows that **09.6 form stars at least as efficiently as typical spiral galaxies**. This **support the AGN positive feedback scenario** that predicts an enhanced star formation activity along the shocked region inside the radio-jets. To accurately determine the SFE in the 09.6 spot, high-resolution interferometric data are required. In order to do so, we have proposed a follow-up with the Plateau de Bure interferometer.

References

Baum, S. A. & Heckman, T. 1989, ApJ, 336, 681

Bell, E. F. & de Jong, R. S. 2001, ApJ, 550, 212

Bicknell, G. V., Sutherland, R. S., van Breugel, W. J. M., et al. 2000, ApJ, 540, 678

Bigiel, F., Leroy, A., Walter, F., et al. 2008, AJ, 136, 2846

Calzetti, D., Kennicutt, R. C., Engelbracht, C. W., et al. 2007, ApJ, 666, 870

Charmandaris, V., Combes, F., & van der Hulst, J. M. 2000, A&A, 356, L1

Daddi, E., Elbaz, D., Walter, F., et al. 2010, ApJ, 714, L118

De Breuck, C., Downes, D., Neri, R., et al. 2005, A&A, 430, L1

Kennicutt, R. C. & Evans, N. J. 2012, ARA&A, 50, 531

Kennicutt, Jr., R. C. 1998, ApJ, 498, 541

Leahy, J. P. & Williams, A. G. 1984, MNRAS, 210, 929

Papadopoulos, P. P., Greve, T. R., Ivison, R. J., & De Breuck, C. 2005, A&A, 444, 813

Roche, N. & Eales, S. A. 2000, MNRAS, 317, 120

Salomé, Q., Salomé, P., & Combes, F. 2014, A&A, submitted
Schiminovich, D., van Gorkom, J. H., van der Hulst, J. M., & Kasow, S. 1994, ApJ, 423, L101
Solomon, P. M., Downes, D., Radford, S. J. E., & Barrett, J. W. 1997, ApJ, 478, 144
Tadhunter, C., Holt, J., Delgado, R. G., et al. 2011, MNRAS, 412, 960
van Breugel, W., Filippenko, A. V., Heckman, T., & Miley, G. 1985, ApJ, 293, 83
van Breugel, W., Fragile, C., Anninos, P., & Murray, S. 2004, IAUS, 217, 472
van Breugel, W. J. M. & Dey, A. 1993, ApJ, 414, 563
Wiklind, T., Combes, F., Henkel, C., & Wyrowski, F. 1997, A&A, 323, 727